Scientific Research Publishing

Journal of Applied Mathematics and Physics, 2019, 7, 271-280
http://www.scirp.org/journal/jamp
ISSN Online: 2327-4379
ISSN Print: 2327-4352

First Principle Study of the Structural and Piezoelectric Properties of Perovskite $ZrTi(PbO_3)_2$ Materials for Naval SONAR

Owolabi Joshua Adeyemi[1], Gidado Mohammed Mawashi[1], Alhassan Shuaibu[2], Bamikole Johnson Akinade[3], Ugbe Raphael Ushiekpan[1]

[1]Department of Physics, Nigerian Defence Academy, Kaduna, Nigeria
[2]Department of Physics, Faculty of Science, Kaduna State University, Kaduna, Nigeria
[3]Department of Physics, Federal University Lafia, Lafia, Nigeria
Email: owolabiy26@gmail.com

How to cite this paper: Adeyemi, O.J., Mawashi, G.M., Shuaibu, A., Akinade, B.J. and Ushiekpan, U.R. (2019) First Principle Study of the Structural and Piezoelectric Properties of Perovskite $ZrTi(PbO_3)_2$ Materials for Naval SONAR. *Journal of Applied Mathematics and Physics*, **7**, 271-280.
https://doi.org/10.4236/jamp.2019.72022

Received: September 27, 2018
Accepted: February 11, 2019
Published: February 14, 2019

Abstract

First principle calculation within the Density Functional Theory (DFT) and Density Functional Perturbation Theory (DFPT) using Local Density Approximation as implemented in Quantum ESPRESSO has been significantly used to investigate the structural and Piezoelectric, properties of Perovskite $ZrTi(PbO_3)_2$. From structural properties calculation, the ground state total energy of −2417.12 eV has been obtained which led to an equilibrium lattice constant of a= 5.620Å for $ZrTi(PbO_3)_2$. Our obtained optimized atomic positions and atomic effective charge shows that the optimized $ZrTi(PbO_3)_2$ is stable and the Piezoelectric stress tensor is calculated using Berry-phase approach within density functional perturbation theory (DFPT). From our calculation, we have obtained the stress tensor elements with values of $d_{1,5}$ = 6.81, $d_{3,1}$ = 1.69, and $d_{3,3}$ = 6.18, which is in agreement with the values obtained for tetragonal $PbTiO_3$.

Keywords

Structural Properties, Perovskite $ZrTi(PbO_3)_2$ Density Functional Theory (DFT), Density Functional Perturbation Theory (DFPT), Local Density Approximation (LDA)

1. Introduction

Perovskite oxides have wide range of structural, electrical and mechanical prop-

erties, making them vital materials for many nanotechnological applications, which controls production particles about nanometric dimensions. The task of nanotechnology is the development and implementation of methods of research and modeling of nanoparticles [1]. A nanoparticle which is made up of nanomaterials is mostly based on dimension than the structures. Thus, the nanomaterials such as nanograins, nanolayers, nanofibers and perovskite can be classified into nanostructures. Nanostructure materials are characterized by different, better properties (e.g. optical, magnetic or mechanical) than their micro- or macro-structural analogues.

The benefits of these materials are connected with new properties of materials that are better in nanoscale [2]. The newly obtained properties of materials differ in respect of the shape and dimensions with both characteristic and physicochemical properties [3] which give the possibilities of using nanomaterials in many branches of military sectors for research [4]. Such research includes Perovskite solid solutions with high piezoelectric response that shows particular interest when employed as sensors in SONAR devices. When such a material is deformed by underwater sound vibrations, it generates an electric field which can then be interpreted by a computer to gain information of depth and distance. This information is crucial for the defense and operation of Naval submarines and vessels [5].

In 1915 to 1940, there was little progress in development of sonar devices. In 1940, the US sonars typically consisted of a magnetostrictive transducer and an array of nickel tubes connected to a 1-foot-diameter steel plate attached back-to-back to a Rochelle salt crystal in a spherical housing. This assembly penetrated the ship hull and was manually rotated to the desired angle. The piezoelectric Rochelle salt crystal had better parameters, but the magnetostrictive unit wasn't much reliable. With this, Early World War II losses prompted rapid research in the field, pursuing both improvements in magnetostrictive transducer parameters and Rochelle salt reliability. a superior alternative, an Ammonium dehydrogenate phosphate (ADP), was found as a replacement for Rochelle salt; the first application was a replacement of the 24 kHz Rochelle-salt transducers. Within nine months, Rochelle salt was obsolete. The ADP manufacturing facility grew from few dozen personnel in early 1940 to several thousands in 1942 [6].

One of the earliest applications of ADP crystals was hydrophones for acoustic mines which crystals were specified for low-frequency cutoff at 5 Hz, withstanding mechanical shock for deployment of aircraft from 3000 m (10,000 ft), and the ability to survive neighboring mines explosions. One of the key features of ADP reliability is that it can keep its parameters even over prolonged storage, and it has a zero aging characteristics. Another application was for acoustic homing torpedoes where two pairs of directional hydrophones were mounted on the torpedo nose, in the horizontal and vertical plane; the different signals from the pairs were used to steer the torpedo left-right and up-down. A countermeasure was developed that targeted the submarine discharged as an effervescent chemical, that made the torpedo goes after the noisier fizzy decoy. The counter-

measure gives a torpedo with active sonar. Since active sonar reveals the presence and position of the operator, and does not allow exact classification of targets, it is used by fast (planes, helicopters) and by noisy platforms (most surface ships) but rarely by submarines. It is typically activated very briefly at intermittent periods to minimize the risk of detection. Consequently, active sonar is normally considered a backup to passive sonar. In aircraft, active sonar is used in the form of disposable sonbuoys that are dropped in the aircraft's patrol area or in the vicinity of possible enemy sonar contacts [7].

Also Passive sonar arrays for submarines can be developed from ADP crystals. The standard US Navy scanning sonar at the end of World War II operated at 18 kHz using an array of ADP crystals that desired longer range and required the use of lower frequencies. The required dimensions were too big for ADP crystals, so in the early 1950s magnetostrictive and barium titanate piezoelectric systems were developed, but these had problems achieving uniform impedance characteristics, and the beam pattern suffered. Barium titanate was then replaced with more stable lead zirconate titanate (PZT), and the frequency was lowered to 5 kHz. The US fleet used this material in the AN/SQS-23 sonar for several decades. The SQS-23 sonar first used magnetostrictive nickel transducers, but these weighed several tons, and nickel was expensive and considered a critical material. After World War II Magnetostrictive transducers were pursued as an alternative to piezoelectric materials. Nickel scroll-wound ring transducers were used for high-power low-frequency operations, with size up to 13 feet (4.0 m) in diameter, probably the largest individual sonar transducers ever. The advantage of metals is their high tensile strength and low input electrical impedance, but they have electrical losses and lower coupling coefficient than PZT, whose tensile strength can be increased [8].

But it has been observed that most of these Perovskite oxides are complex systems with some degree of disorder, making them challenging to study experimentally and theoretically. However, their complexity gives them their favorable properties, highly accurate modeling which captures the essential features of the disordered structure necessary to explain the behavior of current materials and predict favorable compositions for new materials.

Current synthetic aperture sonar (SAS) systems are exploring device technology with broad bandwidth capabilities for improved system performance. Bandwidth for these systems is not only a function of the transducer but transmit system capabilities, such as available power, maximum pulse length, duty cycle, and waveform. Because these systems are designed for UUVs as small as 9 inches in diameter, transmitted systems must be housed with limited interior volume. This places increased performance constraints on the transducer technology. Bandwidth and power capabilities of the transducer are a function of the electromechanical coupling coefficient, mechanical quality factor, and the drive level limits of the material. At nanoscale dimensions, ferroelectrics exhibit almost all the above mentioned behaviors. High-performance nanoscale ferroelectric perovskites are also required for miniaturization of devices and high-density

nonvolatile memory storage. The processes governing the stability of polarization are not entirely understood and are now under intense experimental and theoretical investigation. Recently, a combination of methodological improvements and rise in computer speed has made first-principles calculations a viable tool for understanding these type of complex systems. In particular, the density functional theory (DFT) approach [9] [10] (Hohenberg and Kohn, 1964; Kohn and Sham, 1965) offers a combination of accuracy and computational speed that may reveal the microscopic structure and interactions of complex systems [11] (Grinberg, Cooper, and Rappe, 2002).

As a result of the above stated problems, the main aim of this research work is to use density functional theory (DFT) simulations as implemented in Quantum ESPRESSO code to model and investigate the properties of new Perovskite oxide $ZrTi(PbO_3)_2$ and also to find out if the material can served as potential material for naval sonar applications.

2. Methodology

Density functional theory (DFT) as implemented in Quantum-ESPRESSO package was used to carry out the calculations on Perovskite oxide $ZrTi(PbO_3)_2$. Total energy calculations were performed within the linear density approximation (LDA). The Perdew-Zunger (LDA) exchange-correlation parameterization was used in the calculations. Zr (4s, 4p, 4d), Pb (5d, 6s, 6p), Ti (3s, 3p, 3d, 4s), and (O 2s and 2p) orbitals were treated as valence orbitals. In all case, the atomic core states were calculated relativistically, spin-orbit coupling was ignored, while the valence states were treated semi-relativistically. We have used a special point's for Brillouin-zone samplings with a $12 \times 12 \times 12$ k-point mesh. While for the Berry's phase calculations, we have used the k-space integrations of $8 \times 8 \times 10$ k-point mesh. The results of the calculations were checked for convergence with respect to the number of k points and the plane wave cutoff energy.

In order to obtain the polarization of our compound Perovskite oxide $ZrTi(PbO_3)_2$, we first carried out self-consistent total-energy calculations as mentioned above. Then, the polarization was computed through the Berry-phase approach within DFPT. Different strains were applied in the z direction to compute d_{33}, and different biaxial strains were also applied simultaneously in the x and y directions to compute d_{31} and d_{15} respectively.

3. Results and Discussions

3.1. Structural Properties

Figure 1 shows our stable Perovskite structure $ZrTi(PbO_3)_2$ while Table 1 shows the optimized atomic positions and atomic effective charge of Perovskite $ZrTi(PbO_3)_2$. Since it is known that the energetic of the system supports the most stable crystal parameter with the lowest energy It is confirmed that once the minimum energy and the corresponding most stable parameters is obtained one can also have the most stable structure as shown in Figure 1 for our stable Pe-

rovskite structure $ZrTi(PbO_3)_2$.

The analysis of the convergences with respect to plane-wave energy cutoff, and with respect to *k*-point sampling grids density are the key starting points of any plane-wave self-consisted field (PWSCF) calculations, this is because, a poor convergence test results always resulted in obtaining incorrect converged total energy. Table 2 and Figure 2 illustrates the results for convergence test with respect to kinetic energy cutoff for Perovskite $ZrTi(PbO_3)_2$, while Table 3 and Figure 3 with respect to *k*-points mesh. Clearly shows that the variations in energy cutoff become stabled from 28 Ry, and therefore increasing the energy cut-off from 28 Ry to 40 Ry does not have much effect on the total energy.

However, in Table 3 and Figure 3 the total energy is independent of the number of *k*-points at a certain points, showing well converged values. The energy changes considerably as the number of *k*-point changed, up to a particular points where it remains unchanged. For instance, increasing the number of *k*-points from $8 \times 8 \times 8$ to $12 \times 12 \times 12$ does not lower the total energy, but gives similar results. The Monkhorst and Pack method of selecting *k*-points widely

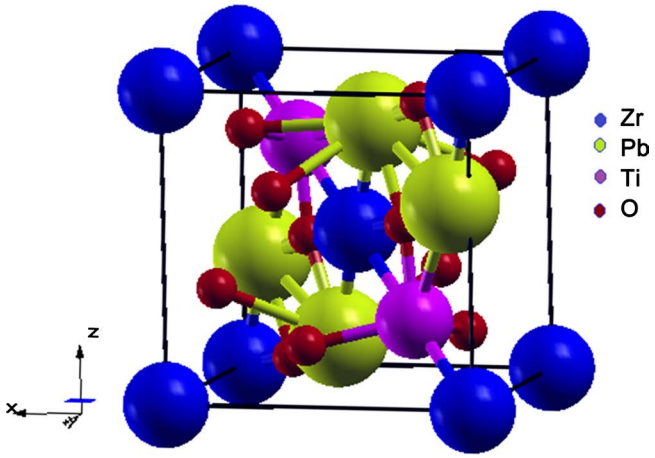

Figure 1. Optimized stable crystal structure of Perovskite $ZrTi(PbO_3)_2$.

Table 1. The calculated optimized atomic positions for Perovskite $ZrTi(PbO_3)_2$. Our optimization is within the linear density approximation LDA.

Atom	*x*	*y*	*z*
Zr	0.000000000	0.000000000	0.000000000
Ti	0.500000000	0.500000000	0.500000000
Pb	0.729799147	0.829605131	0.729799147
Pb	0.270200853	0.170394869	0.270200853
O	0.756926987	0.249398040	0.339505879
O	0.339505879	0.249398040	0.756926987
O	0.839916652	0.421491919	0.839916652
O	0.243073013	0.750601960	0.660494121
O	0.660494121	0.750601960	0.243073013

Table 2. Convergence test result with respect to Kinetic Energy Cutoff

S/N	E_{CUT} (Ry)	E_{TOT} (Ry)
1	12	−2391.11794851
2	16	−2405.62513615
3	20	−2412.08433421
4	24	−2415.06686281
5	28	−2416.41157927
6	32	−2416.43214121
7	36	−2417.28052871

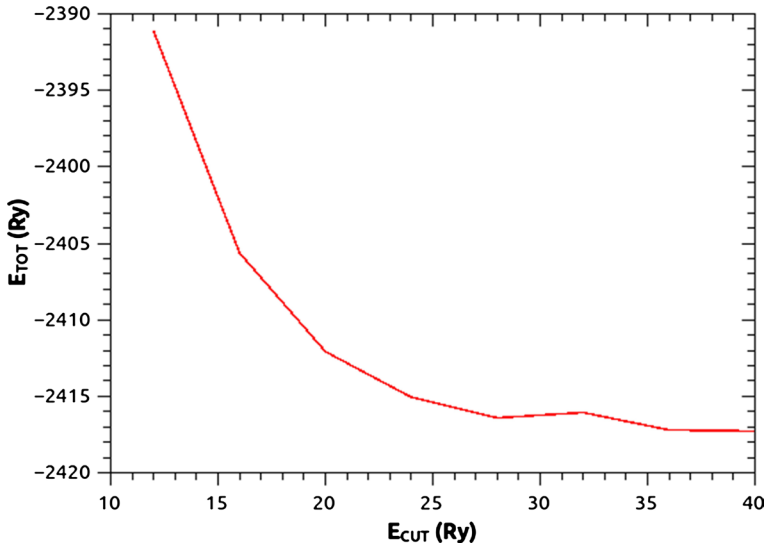

Figure 2. Graph of Convergence test result with respect to Kinetic Energy Cutoff.

Table 3. Convergence test result with respect to K-point mesh

S/N	K-point	E_{TOT} (Ry)
1	2× 2×2	−2391.11794851
2	4× 4×4	−2405.62513615
3	6× 6×6	−2412.08433421
4	8× 8×8	−2415.06686281
5	10× 10×10	−2416.41157927
6	12× 12×12	−2416.43214121

used in most DFT calculations is used in this research [12]. (Monkhorst and Pack, 1976). One of the basic ideas used in this method is to specify the number of *k*-points that are to be used in each direction in reciprocal space. In this work, the 8 × 8 × 8 *k* points was adopted for Perovskite $ZrTi(PbO_3)_2$, since the super-cell approach used have the same length along each lattice vectors, which is also assume to be the same with the reciprocal lattice vector, and therefore this is the reason why 8 × 8 × 8 *k*-points are used in each direction. However, by considering

the idea of numerical integration, it is expected that using the higher *k*-points for example, 12 × 12 × 12 *k*-points will give a more accurate result than a calculation using 8 × 8 × 8 *k*-points but it will be time consuming.

The best way of choosing specific *k*-points points to be use in practice is by computing the calculated total energies together with the selected number of *k*-points on convergence graph. In this situation, it can be seen that with the increasing number of k points, for instance, from 2 × 2 × 2 k points to 8 × 8 × 8 k points, the total energy of the system is (almost) continuously dependent on the number of *k*-points. But, when the *k*-points are increased from 8 × 8 × 8 *k*-points to 12 × 12 × 12 *k*-points, the total energy is seen to be independent of the number of *k*-points.

Also as an initial step of understanding the structural properties of any material, the total energy was calculated as a function of the lattice constant for Perovskite $ZrTi(PbO_3)_2$. The energy versus lattice constant data is plotted in Figure 4.

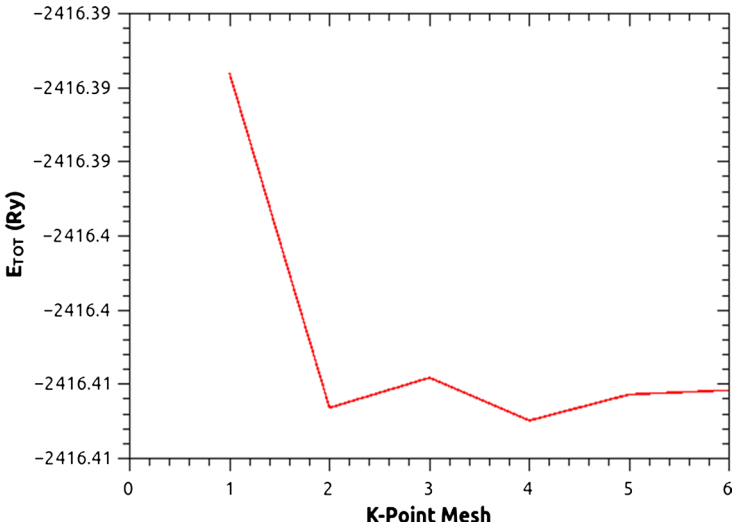

Figure 3. Convergence test with respect to K-point mesh.

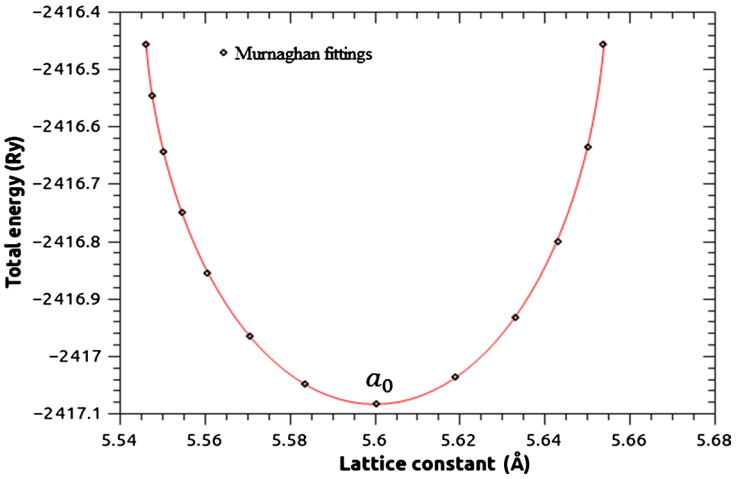

Figure 4. Structural optimization plots of our Perovskite $ZrTi(PbO_3)_2$ all calculations are within the LDA-DFT.

To extract the value of a_0 from any DFT calculations, it is important to think about the functional form of $E_{\text{tot}}(a)$. One of the simplest methods is to express the total energy using a truncated Taylor expansion:

$$E_T(a) \approx E_T(a_0) + \alpha(a, a_0) + \beta(a, a_0) \tag{1}$$

with $\alpha = \mathrm{d}E/\mathrm{d}a\big|_{a_0}$ and $\beta = \frac{1}{2}\mathrm{d}^2E/\mathrm{d}a^2\big|_{a_0}$.

By definition, if a_0 is the lattice parameter corresponding to the minimum energy, that can fit our numerical data to

$$E_T(a) \cong E_0 + \beta(a, a_0)^2 \tag{2}$$

where E_0, β, a_0 are treated as fitting parameters. Even though we have treated β as a fitting parameter in equation 1, the graph of **Figure 4**, shows that a_0 = 5.6 Å, this indicate that the value is greater than the equilibrium lattice parameter of cubic Perovskite $PbTiO_3$ [14] [15], the differences may arise due to the presents of Zr in the cubic Perovskite $ZrTi(PbO_3)_2$ or using LDA functional in our calculations as GGA-PBE functional adopted in their calculations has proved to always overestimate the lattice parameters [13]. **Table 4** shows the summarized optimized results with the results of similar materials for comparison.

Therefore, for our Perovskite $ZrTi(PbO_3)_2$ one can clearly see that the bulk modulus at the fully relaxed state is comparable with the other results of similar materials obtained by [11] [15].

Table 4 Also shows the optimized atomic positions and atomic effective charge of Perovskite $ZrTi(PbO_3)_2$. Since it is known that the energetic of the system supports the most stable crystal parameter with the lowest energy.

3.2. Piezoelectric Properties

Using the fully-relaxed structures, the piezoelectric tensor is determined by the density-functional perturbation theory (DFPT). In the present study, we calculate the piezoelectric strain constants which connects the induced polarization P_{i} and strain tensor element as

$$d_{ijk} = \frac{\partial P_i}{\partial \varepsilon_{jk}} \tag{5}$$

where we computed P_i using Berry phase method as a function of strain as

Table 4. Calculated lattice parameters and bulk moduli of our Perovskite $ZrTi(PbO_3)_2$. with $BaTiO_3$ and $PbTiO_3$ for comparisons.

Piezoelectric materials	Lattice constants (Å)			Bulk modulus (GPa)		
	This work	Theory	Expt.	This work	Theory	Expt.
$ZrTi(PbO_3)_2$ ($a = b = c$).	5.620	5.544	---	189.56	170.55	--
$BaTiO_3$ ($a = b = c$)	---	3.977	4.000	-	178.65	195.00
$PbTiO_3$ ($a = b = c$)	---	3.966	3.930	-	173.21	195.00

Table 5. Comparisons of our calculated Piezoelectric stress tensor elements (C/m^2) of ferroelectric $ZrTi(PbO_3)_2$, with that of tetragonal $PbTiO_3$ Obtained by (Min, Sang, Cheeyoung and Hee, 2015).

Materials	Method	$d_{1,5}$	$d_{3,1}$	d_{33}
$ZrTi(PbO_3)_2$	DFT-LDA	6.81	1.69	6.18
$PbTiO_3$	DFT-LDA	6.73	1.68	6.14
$PbTiO_3$	GGA-PBEsol	3.68	1.49	3.94

implemented in QE code, Wu and Cohen applied the same method for piezoelectricity of $PbTiO_3$. For our Perovskite $ZrTi(PbO_3)_2$, we have noticed that the polarization is along (001) axis, which is in agreement with the results obtained in case of $PbTiO_3$ therefore to describe the piezoelectric effects in our compound we computed three piezoelectric constants $\left(d_{3,1}=d_{3,2}\right)$, $d_{3,3}$ and $\left(d_{1,5}=d_{2,4}\right)$.

Additionally, $\left(d_{3,1}=d_{3,2}\right)$ and $d_{3,3}$ describe the zero field polarization induced along the z-axis when crystal is uniformly strained in the basal xy-plane or along the z-axis, respectively. **Table 5** gives our computed results together with that obtained value of Perovskite $PbTiO_3$ for comparison [12].

As shown in **Table 5**, our obtained values are in good agreement with the LDA values of single crystal $PbTiO_3$. However, there is consistently larger difference with those of GGA as expected.

4. Conclusions

We have successfully used First principle theory to contribute significantly to our understanding and systematically presented a theoretical study of the structural, piezoelectric properties of the Perovskite $ZrTi(PbO_3)_2$ materials based on Density Functional Theory (DFT) and Density Functional Perturbation Theory (DFPT) within Local Density Approximation.

The ground state total energy of −2417.12 eV is obtained which gives the stable structure of the Perovskite $ZrTi(PbO_3)_2$ material with an equilibrium lattice constant of a = 5.620Å. The optimized atomic positions of Perovskite $ZrTi(PbO_3)_2$ shows that our optimization is within the linear density approximation (LDA). Also our calculated Piezoelectric stress tensor elements of ferroelectric $ZrTi(PbO_3)_2$, gives $d_{1,5}$ = 6.81, $d_{3,1}$ = 1.69, and $d_{3,3}$ = 6.18, which is in agreement with the values obtained in tetragonal $PbTiO_3$.

Conflicts of Interest

The authors declare no conflicts of interest regarding the publication of this paper.

References

[1] Maynard, A.D., Aitken, R.J., Butz, T., Colvin, V., Donaldson, K., Oberdörster, G. and Tinkle, S.S. (2006) Safe Handling of Nanotechnology. *Nature*, **444**, 267. https://doi.org/10.1038/444267a

[2] Corley, E.A., Scheufele, D.A. and Hu, Q. (2009) Of Risks and Regulations: How Leading US Nanoscientists Form Policy Stances about Nanotechnology. *Journal of Nanoparticle Research*, **11**, 1573-1585. https://doi.org/10.1007/s11051-009-9671-5

[3] Kreyling, W.G., Semmler-Behnke, M. and Chaudhry, Q. (2010) A Complementary Definition of Nanomaterial. *Nano Today*, **5**, 165-168. https://doi.org/10.1016/j.nantod.2010.03.004

[4] Geszke-Moritz, M., Clavier, G., Lulek, J. and Schneider, R. (2012) Copper- or Manganese-Doped ZnS Quantum Dots as Fluorescent Probes for Detecting Folic Acid in Aqueous Media. *Journal of Luminescence*, **132**, 987-991. https://doi.org/10.1016/j.jlumin.2011.12.014

[5] Friedman, N. (1995) US Submarines through 1945: An Illustrated Design History. Naval Institute Press, 259-260.

[6] Frank, M. (2015) Sonar Tranducers: A History Archived at the Wayback Machine.

[7] Moffatt, I. (2005) Mines and Minesweeping Techniques of WW2.

[8] Massa, F. (2015) Sonar Transducers: A History World War II Prompted Incredible A Complishments-Aided by Eliminating Red Tape: Rapid Advances in Production Engineering.

[9] Hohenberg, P. and Kohn, W. (1964) Inhomogeneous Electron Gas. *Physical Review*, **136**, B864. https://doi.org/10.1103/PhysRev.136.B864

[10] Kohn, W. and Sham, L.J. (1965) Self-Consistent Equations including Exchange and Correlation Effects. *Physical Review*, **140**, A1133. https://doi.org/10.1103/PhysRev.140.A1133

[11] Grinberg, I., Cooper, V. R., & Rappe, A. M. (2002). Relationship between local structure and phase transitions of a disordered solid solution. *Nature*, 419(6910n), 909. https://doi.org/10.1038/nature01115

[12] Monkhorst, H.J. and Pack, J.D. (1976) Special Points for Brillouin-Zone Integrations. *Physical Review B*, **13**, 5188.

[13] Pfrommer, B.G., Cote, M., Louie, S.G. and Cohen, M.L. (1997) Relaxation of Crystals with the Quasi-Newton Method. *Journal of Computational Physics*, **131**, 233. https://doi.org/10.1006/jcph.1996.5612

[14] Mabud, S.A. and Glazer, A.M. (1979) Lattice Parameters and Birefringence in $PbTiO_3$ Single Crystals. *Journal of Applied Crystallography*, **12**, 49-53. https://doi.org/10.1107/S0021889879011754

[15] Kim, M.C., Lee, S.G., Joh, C. and Seo, H.S. (2016) First-Principles Predictions of Structures and Piezoelectric Properties of $PbTiO_3$ Single Crystal. *Transactions on Electrical and Electronic Materials*, **17**, 29-32. https://doi.org/10.4313/TEEM.2016.17.1.29